

Does sunlight always accelerate water droplet evaporation? F

Cite as: Appl. Phys. Lett. **116**, 253903 (2020); <https://doi.org/10.1063/5.0012700>

Submitted: 05 May 2020 . Accepted: 08 June 2020 . Published Online: 26 June 2020

Xiongjiang Yu , and Jinliang Xu 

COLLECTIONS

F This paper was selected as Featured



View Online



Export Citation



CrossMark

Lock-in Amplifiers
up to 600 MHz



Does sunlight always accelerate water droplet evaporation?



Cite as: Appl. Phys. Lett. **116**, 253903 (2020); doi: [10.1063/5.0012700](https://doi.org/10.1063/5.0012700)

Submitted: 5 May 2020 · Accepted: 8 June 2020 ·

Published Online: 26 June 2020



View Online



Export Citation



CrossMark

Xiongjiang Yu^{1,2} and Jinliang Xu^{1,a)}

AFFILIATIONS

¹Beijing Key Laboratory of Multiphase Flow and Heat Transfer for Low Grade Energy Utilization and Key Laboratory of Power Station Energy Transfer Conversion and System of Ministry of Education, North China Electric Power University, Beijing 102206, People's Republic of China

²Department of Energy and Process Engineering, Norwegian University of Science and Technology, Trondheim 7491, Norway

^{a)}Author to whom correspondence should be addressed: xjl@ncepu.edu.cn

ABSTRACT

We investigate droplet evaporation, which is a natural phenomenon but the mechanism is not well understood. We are surprised to find that sunlight irradiation does not always enhance droplet evaporation, which is against the common sense that “Sun accelerates water evaporation.” This is true at least for short-time evaporation. A whole droplet lifetime consists of two regimes of evaporation: a light induced deterioration regime and an acceleration regime. The deterioration regime is explained by the decreased temperature difference from the droplet bottom to apex, weakening Marangoni flow to hinder conduction heat transfer from the substrate to the droplet. The enhanced regime is explained by the reduced light energy reflection via the droplet surface. The substrate conduction heat transfer and radiation heat transfer of light are coupled to dominate evaporation. The two mechanisms create opposite contributions, resulting in a constant evaporation rate for sunlight irradiation on a droplet. However, natural light decreases the evaporation rate vs time. Hence, evaporation rates with and without sunlight irradiation cross at a specific time. Our work enhances the fundamental understanding of droplet evaporation and provides a useful guideline for efficient solar energy utilization.

Published under license by AIP Publishing. <https://doi.org/10.1063/5.0012700>

Solar energy drives global water circulation due to energy absorption in the visible and infrared (IR) spectrum. The optothermal effect warms up water and its surrounding environment to accelerate water evaporation and vapor diffusion. Inspired by such a natural phenomenon, light-matter interactions have been widely investigated, including the development of micro/nanostructures for efficient light energy absorption^{1–7} and enhanced plasmonic heating.^{8–12} Even though sunlight driven droplet evaporation is a daily encountered phenomenon, the associated mechanism is not well understood yet. Here, we investigate light induced droplet evaporation. The droplet was positioned on the tip of a capillary tube, which is optical transparent and called the substrate. Here, the substrate includes the capillary tube and water in the capillary hole. The protruding part is the droplet, which is of interest to us. A xenon lamp emits parallel light, having a similar optical spectrum to natural sunlight. The droplet surface temperatures from the droplet apex to the contact line were measured using an infrared (IR) camera. During the early stage of droplet dynamics, we are surprised to find that droplet evaporation rates under light irradiation are smaller than those under natural light conditions, indicating

the deteriorated droplet evaporation by sunlight. This finding is against the common sense that “sunlight accelerates water evaporation.” Indeed, the latter evaporation stage possesses higher evaporation rates with the help of light irradiation. We conclude two mechanisms of light induced heating and substrate induced heat conduction, which are coupled to dominate droplet evaporation.

To explore the effect of sunlight irradiation on droplet evaporation, a careful experiment was performed. Filling water in the capillary tube eventually forms a droplet above the hole (see Fig. S1 in the [supplementary material](#)). We note that there are two modes of droplet evaporation: constant contact area mode and constant contact angle mode.^{13–17} The hole structure ensures the constant contact area mode, under which the project area of the droplet under parallel light irradiation is not changed during droplet lifetime. Because the light intensity significantly decays after passing through an optical length of \sim mm scale,¹² the hole depth has a weak influence on evaporation, but the hole diameter affects droplet formation. To stack a droplet on the substrate, the hole diameter of 1.0 mm is used, significantly smaller than the capillary length of water.

To explain why sunlight irradiation deteriorates droplet evaporation, a high-speed camera captures the droplet morphology. A set of independent experiment runs were arranged, with each run corresponding to a contact angle range from $CA + \delta$ to $CA - \delta$, where CA is the average contact angle and δ is the contact angle deviation. $CA + \delta$ and $CA - \delta$ are called the starting and ending conditions, respectively. The time period is recorded as Δt during the variation of contact angles in such a range. Typically, Δt is the minute scale. The droplet evaporation rate is $E_r = \Delta V/\Delta t$, where ΔV is the droplet volume change. Here, the selection of CA as the controllable variable is due to its important domination in evaporation. CA not only influences Marangoni flow to affect heat transfer from the substrate to the droplet but also influences light energy reflection via the droplet surface. Besides, CA is easy to be controlled in the experiment. Figure 1 shows increased evaporation rates when contact angles are increased, which are true for conditions with and without sunlight irradiation. Light irradiation with $q_r = 1.3 \text{ kW/m}^2$ shows apparently smaller evaporation rates than natural light conditions with $q_r = 0$. For natural light irradiation, a larger contact angle yields a larger droplet height and volume. The former establishes Marangoni flow to enhance heat transfer from the droplet bottom to apex. Consequently, heat conduction from the substrate to the droplet bottom is also enhanced. Meanwhile, a larger droplet volume has a large surface area exposed to air to accelerate mass transfer from liquid to vapor. The above two factors cause higher evaporation rates at larger contact angles. The light induced evaporation in a short-time period also displays the rise trend vs contact angles. We record V_0 as the droplet volume at $CA = 90^\circ$ and find that the difference between starting CA and ending CA

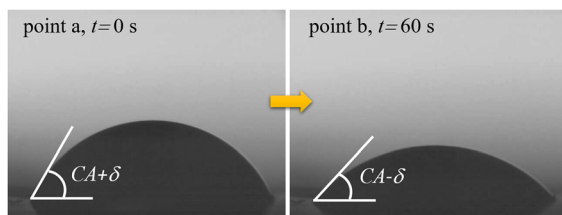
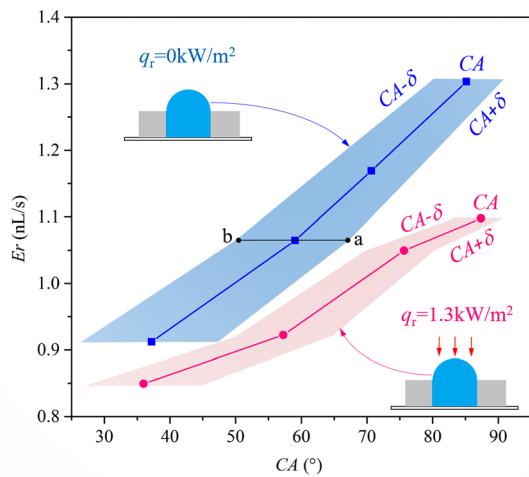


FIG. 1. Effect of contact angles on the suppression of short-time droplet evaporation by sunlight irradiation.

decreases at a higher evaporation rate, which is caused by the nonlinear geometry relationship between V and CA . For example, V changes from V_0 to $0.77V_0$ ($\Delta V = 0.23V_0$) with CA changed from 90.0° to 79.6° (10.4° difference), but V changes from $0.58V_0$ to $0.38V_0$ ($\Delta V = 0.2V_0$) with CA changed from 67.8° to 50.2° (17.6° difference). We note that the instantaneous evaporation rate is represented by an average value in a small contact angle range such as 10° . A more accurate method is to supply water to compensate the contact angle variation, which is difficult to do this due to the very small change of water in the short-time evaporation test.

Figures 2–4 identify droplet surface temperatures, which explain the data trend shown in Fig. 1. The IR camera measurement covers both the droplet domain and vapor boundary domain. An important issue is to locate the droplet surface position in the temperature image. The determination principle is described as follows: For the water surface temperature measurement, the IR camera detects the infrared

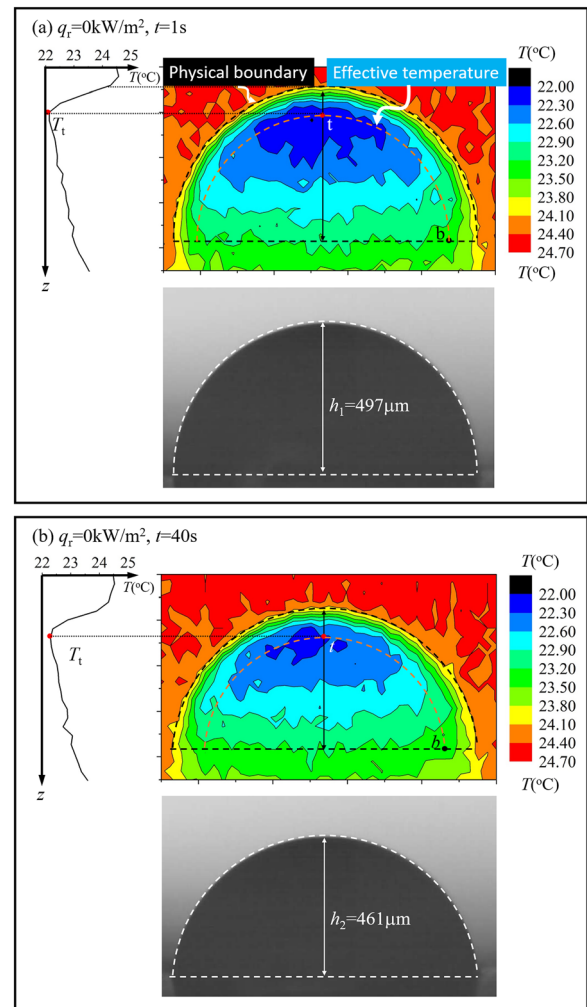


FIG. 2. The IR measured temperatures and droplet morphology measured using a high-speed camera for droplet evaporation without light irradiation at (a) $t = 1 \text{ s}$ and (b) $t = 40 \text{ s}$.

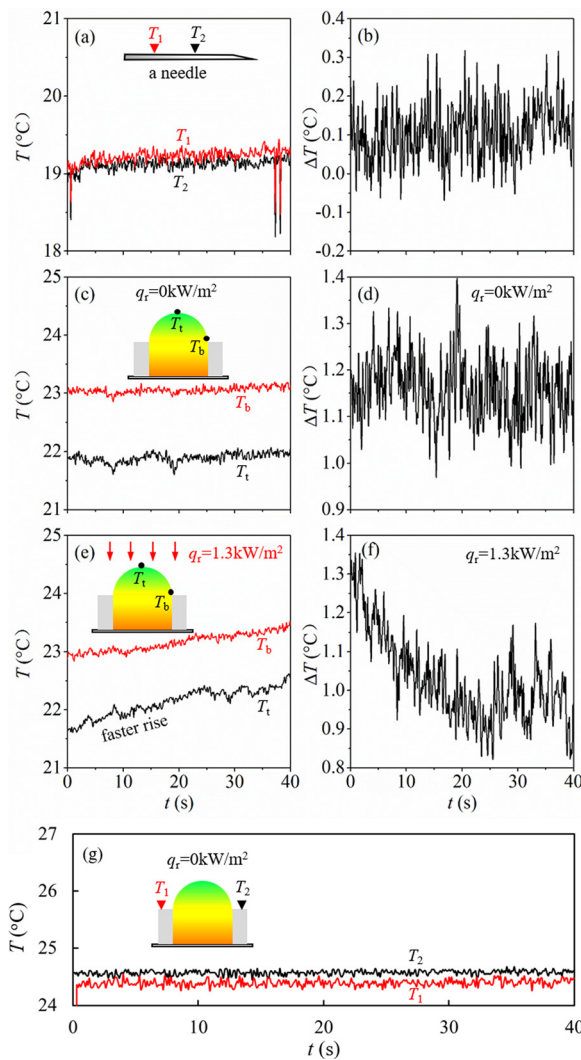


FIG. 3. Transient temperatures and temperature difference [(a) and (b) on two points of a needle surface, (c) and (d) for droplet evaporation with $q_r = 0$, (e) and (f) for droplet evaporation with $q_r = 1.3 \text{ kW/m}^2$, and (g) on two points of the capillary tube tip].

energy signal emitted from a thin liquid film thickness of $\sim 300 \mu\text{m}$.¹² Because the test droplet has a size of $\sim 1 \text{ mm}$, the temperature measurement in the droplet domain is sufficiently accurate. Because the surface of an $\sim \text{mm}$ scale droplet has a thickness of $\sim 10 \mu\text{m}$, which is significantly thinner than $\sim 300 \mu\text{m}$, the IR detection of droplet surface temperature includes the background signal effect. Fortunately, the background signal does not influence the determination of the droplet surface. This is because when crossing the vapor boundary layer from the vapor side to the liquid side, the lowest temperature always exists at the droplet surface,^{11,12} based on which the droplet surface can be determined. Examples are shown in Fig. 2(a) at $t = 1 \text{ s}$ and Fig. 2(b) at $t = 40 \text{ s}$ under natural light conditions. In Fig. 2, temperature distributions along the vertical coordinate and in the whole domain, as well as the droplet morphology, are demonstrated. The droplet apex, also

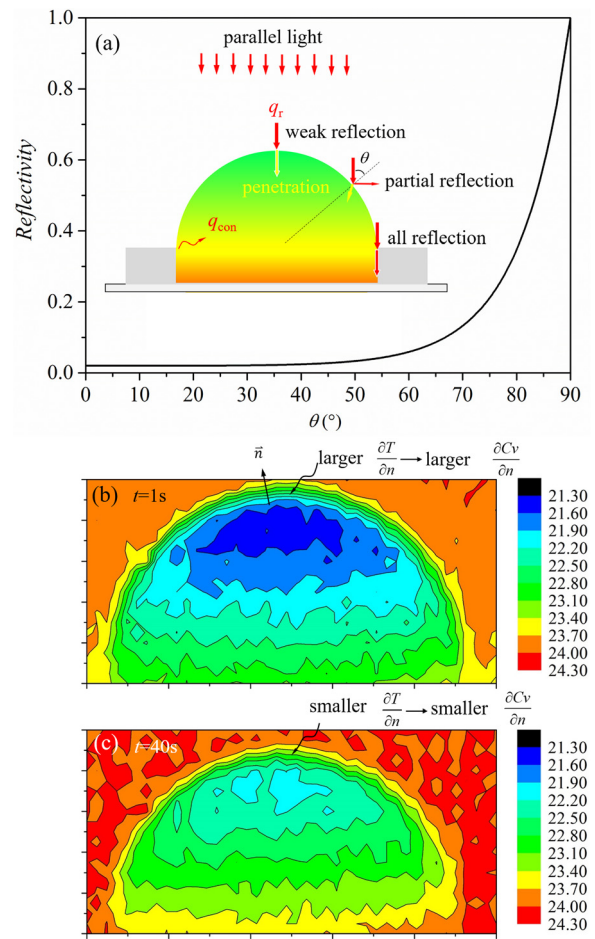


FIG. 4. Light reflectivity on the droplet surface (a) and temperature distribution on the droplet and vapor boundary layer with $q_r = 1.3 \text{ kW/m}^2$ at (b) $t = 1 \text{ s}$ and (c) $t = 40 \text{ s}$.

called the top point t , is interest to us. Temperatures at the bottom (contact line) T_b are larger than the droplet apex T_t , yielding a temperature difference $\Delta T = T_b - T_t$.

How to generate a temperature difference is discussed here. Considering a droplet in natural light, the vapor concentration gradient in the vapor boundary creates mass transfer from the droplet to the environment, resulting in lower droplet temperature than the environment, which is called the evaporation induced refrigeration effect. This mass transfer also establishes a temperature difference from the droplet bottom to apex, which is scaled as $\Delta T = \frac{J \Delta H_{\text{vap}} h_0}{K_L}$,¹⁸ where J is the evaporation mass flux, ΔH_{vap} is the latent heat of evaporation, h_0 is the droplet height, and K_L is the thermal conductivity of liquid. In this Letter, for a droplet having a contact radius of $500 \mu\text{m}$, $CA = 90^\circ$, $h_0 = 500 \mu\text{m}$, $\Delta H_{\text{vap}} = 2457 \text{ kJ/kg}$, $K_L = 0.628 \text{ W/mK}$, and $J = 0.828 \text{ g/m}^2 \text{ s}$ like those encountered in Fig. 1, the estimated temperature difference is $\Delta T = 1.6^\circ\text{C}$, which roughly agrees with the measured value of 1.2°C in Fig. 2. The 0.4°C difference between theoretical prediction and measurement is caused by the treatment of droplet apex temperature T_t . As mentioned already, the droplet surface temperature

measurement may contain the background signal due to the surface thickness significantly less than $300\ \mu\text{m}$, decreasing the measurement accuracy of T_t . To overcome this difficulty, T_t is measured by a couple of pixels away from the droplet surface, pointing the inside droplet direction, noting that a pixel corresponds to $33\ \mu\text{m}$ resolution for the IR measurement. This overestimates T_t to slightly decrease the measured ΔT .

For short-time evaporation, it is necessary to check the time dependent temperatures. Before doing this, the temperatures at two points on a needle surface are detected. The two temperatures are almost identical, and the difference between the two points is around $0.1\ ^\circ\text{C}$ [see Figs. 3(a) and 3(b)]. For natural light conditions ($q_r = 0$), both T_b and T_t are stable vs time and ΔT is kept around $\sim 1.2\ ^\circ\text{C}$ [see Figs. 3(c) and 3(d)]. The situation is changed for sunlight irradiation with $q_r = 1.3\ \text{kW/m}^2$. Covering a time period of 40 s, both T_t and T_b increase vs time. However, T_t increases faster than T_b , decreasing the temperature difference $\Delta T = T_b - T_t$ from 1.2 to $1.3\ ^\circ\text{C}$ at the beginning to $\sim 0.9\ ^\circ\text{C}$ at 25–40 s [see Figs. 3(e) and 3(f)]. One notes that Marangoni flow in a droplet is related to the temperature difference.¹⁹ Under the natural light condition, the $\sim 1.2\ ^\circ\text{C}$ temperature difference is sufficient to establish the Marangoni flow, but sunlight irradiation decreases the temperature difference to weaken Marangoni flow. The temperatures on the SiO_2 capillary tube tip are stable vs time during droplet evaporation [see Fig. 3(g)].

Figure 4 explains the faster rise of T_t . Part of energy is reflected for parallel light irradiation on a droplet. During reflection, incident light and reflected light are in the same plane, called the incident plane. The s polarization refers to the polarization of the electric field normal to the incident plane, and the magnetic field is in the incident plane. The p polarization refers to the polarization of the electric field in the incident plane, and the magnetic field is normal to the incident plane. For s and p polarizations, the light reflectivity is $R_s = \left(\frac{\sin(\theta - \theta_e)}{\sin(\theta + \theta_e)}\right)^2$ and $R_p = \left(\frac{\tan(\theta - \theta_e)}{\tan(\theta + \theta_e)}\right)^2$, respectively,²⁰ where θ , θ_e are the incident angle and exit angle, respectively. Assuming the same irradiation power of s and p polarizations, the effective reflectivity R_f on the droplet surface is $R_f = \frac{1}{2}(R_s + R_p)$. Figure 4(a) shows smaller R_f for θ smaller than 50° – 60° , but it sharply increases beyond 50° – 60° . This means that most of light energy is absorbed at the droplet apex, but almost all the energy is reflected at the droplet contact line, explaining the faster rise of T_t .

The faster rise of T_t decreases ΔT , weakening Marangoni flow to decrease heat transfer for evaporation. This conclusion is verified by examining the vapor concentration (C_v) in the vapor boundary layer. Because C_v is not known, an analogy is established between mass transfer and heat transfer using the Lewis Number $Le = \alpha/D$, where α and D are the thermal diffusion coefficient and mass diffusion coefficient of water–vapor, respectively. Taking $\alpha = 0.22\ \text{cm}^2/\text{s}$ and $D = 0.24\ \text{cm}^2/\text{s}$ at a room temperature of $24.6\ ^\circ\text{C}$ and 1 atm pressure gives $Le = 0.92 \sim 1$. This scale law indicates that the vapor concentration gradient can be represented by the temperature gradient in the vapor boundary. Figure 4(b) shows the larger temperature gradient $\frac{\partial T}{\partial n}$ to indicate the larger heat transfer rate, where n is normal to the droplet surface after a short time of light irradiation of 1 s, which is similar to that without light irradiation. Similarity analysis indicates larger mass transfer in the vapor boundary layer. After a time irradiation of

40 s, $\frac{\partial T}{\partial n}$ obviously decreases to show the deteriorated heat/mass transfer in the vapor boundary layer [see Fig. 4(c)].

Figure 5 shows the crossover phenomenon of droplet evaporation with and without sunlight irradiation, with Fig. 5(a) for V - t curves and Fig. 5(b) for evaporation rates $-dV/dt$. The natural light condition is examined first, which shows a nonlinear V - t distribution. A parabolic curve fitting matches measured data, leading to a linear decrease in evaporation rates, which agrees with the instantaneous measurements of Er shown in Fig. 1. With time evolution, the decreased contact angle is the reason to reduce evaporation rates. However, for sunlight irradiation, a perfect linear variation of V - t is observed, yielding a constant evaporation rate during whole droplet lifetime. At any time, the total heat transfer rate Q_t consists of a substrate conduction part Q_c and a light energy absorption part Q_r : $Q_t = Q_c + Q_r$. The two components have opposite variation trends with respect to time. Q_c reduces vs time, which is due to the decreased droplet height to weaken Marangoni flow. On the other hand, Q_r increases vs time, which is due to the decreased light reflection via the droplet surface. A more flattened surface causes less reflection and ensures more absorption of light energy [see Fig. 4(a)]. The constant evaporate rate is explained by the comprehensive effect of Q_c and Q_r . Thus, the decreased evaporation rate without sunlight irradiation and

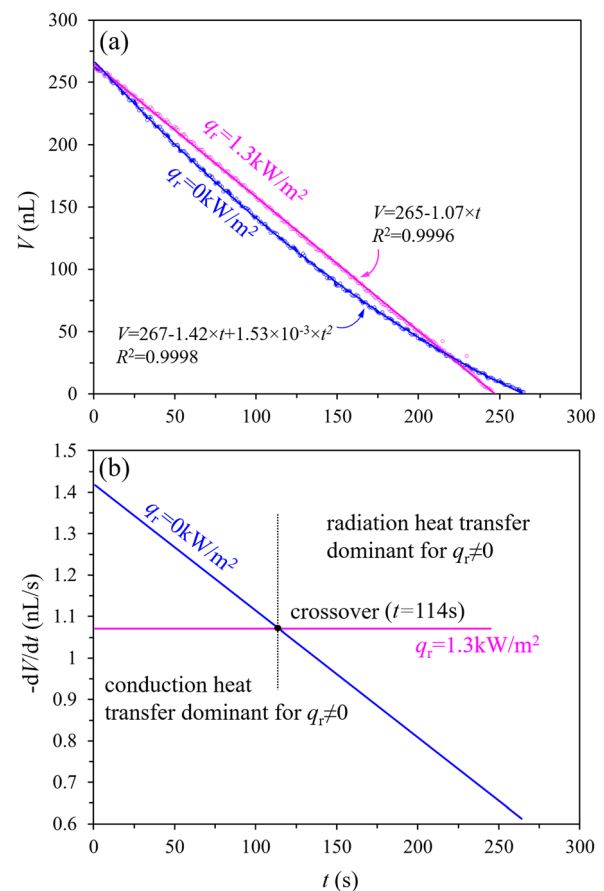


FIG. 5. The crossover phenomenon with and without sunlight irradiation [(a) V - t curves and (b) evaporation rate curves].

the constant evaporation rate with sunlight irradiation have a crossing point at $t = 114$ s. For sunlight irradiation, evaporation rates display two regime distributions: a conduction heat transfer dominant regime before the crossing point and a radiation heat transfer dominant regime beyond the crossing point.

In summary, we identify two regimes of droplet evaporation under sunlight irradiation and conclude that sunlight does not always enhance droplet evaporation, breaking through the common sense that Sun accelerates water evaporation. This is true at least in the early evaporation stage. The light enhanced evaporation occurs at the latter stage. Our work explains the observed phenomenon. The light deteriorated evaporation is caused by the decreased temperature difference between the droplet bottom and top; thus, Marangoni flow is weakened to hinder the heat transfer from the substrate to the droplet. The light enhanced evaporation is caused by the reduced light energy reflection via the droplet surface. Our finding enhances the fundamental understanding of the natural phenomenon and provides a guideline for efficient energy utilization for seawater desalination and vapor generation. The contact angle is an important parameter. For heat supply by substrate conduction only, evaporation is preferable with a larger droplet contact angle. Alternatively, if one uses solar energy, evaporation is preferable on a flattened liquid film, under which less light energy is reflected. Our finding provides a guideline to make a constant evaporation rate for humidity control, which is important to be used in small space volume. Because pure water is used, only the infrared energy is absorbed without using the visible spectrum band. The droplet array can be stacked on a set of solid cavities or capillary tube tips, just like encountered in this study. As the parallel light source, sunlight shall irradiate droplets from top in the direction normal to the substrate bottom plane to keep the evaporation rate constant.

See the [supplementary material](#) for the details of the experimental setup and process.

We appreciate the funding support from the Natural Science Foundation of China (Nos. 51821004 and 51806065) and Fundamental Research Funds for Central Universities (No. 2020DF002).

DATA AVAILABILITY

The data that support the findings of this study are available from the corresponding author upon request.

REFERENCES

- ¹D. Li, A. Li, Y. Chen, G. Chen, X. Chen, D. Zhang, H. Zhu, I. A. Samo, and H. Song, *Carbon* **162**, 481 (2020).
- ²M. Gao, L. Zhu, C. K. Peh, and G. W. Ho, *Energy Environ. Sci.* **12**, 841 (2019).
- ³G. Liu, J. Xu, and K. Wang, *Nano Energy* **41**, 269 (2017).
- ⁴T. Chen, W. Wang, T. Tao, A. Pan, and X. Mei, *Appl. Surf. Sci.* **509**, 145182 (2020).
- ⁵Y. Hu, L. Mao, X. Guan, K. A. Tucker, H. Xie, X. Wu, and J. Shi, *Renewable Sustainable Energy Rev.* **119**, 109527 (2020).
- ⁶Y. Pan, X. Yuan, L. Jiang, H. Yu, J. Zhang, H. Wang, R. Guan, and G. Zeng, *Chem. Eng. J.* **354**, 407 (2018).
- ⁷C. Tang, H. Bai, L. Liu, X. Zan, P. Gao, D. D. Sun, and W. Yan, *Appl. Catal., B* **196**, 57 (2016).
- ⁸L. D. Sio, T. Placido, R. Comparelli, M. L. Curri, M. Striccoli, N. Tabiryan, and T. J. Bunning, *Prog. Quantum Electron.* **41**, 23 (2015).
- ⁹H. Jin, G. Lin, L. Bai, A. Zeiny, and D. Wen, *Nano Energy* **28**, 397 (2016).
- ¹⁰G. Liu, H. Cao, and J. Xu, *Sol. Energy* **170**, 184 (2018).
- ¹¹J. Xu, X. Yan, G. Liu, and J. Xie, *Nano Energy* **57**, 791 (2019).
- ¹²X. Yan, J. Xu, Z. Meng, J. Xie, and G. Liu, *Langmuir* **36**, 1680 (2020).
- ¹³R. G. Picknett and R. Bexon, *J. Colloid Interface Sci.* **61**, 336 (1977).
- ¹⁴C. Bourges-Monnier and M. E. R. Shanahan, *Langmuir* **11**, 2820 (1995).
- ¹⁵S. A. Kulinich and M. Farzaneh, *Appl. Surf. Sci.* **255**, 4056 (2009).
- ¹⁶D. I. Yu, H. J. Kwak, S. W. Doh, H. S. Ahn, H. S. Park, M. Kiyofumi, and M. H. Kim, *Langmuir* **31**, 1950 (2015).
- ¹⁷G. McHale, S. M. Rowan, M. L. Newton, and M. K. Banerjee, *J. Phys. Chem. B* **102**, 1964 (1998).
- ¹⁸R. G. Larson, *AIChE J.* **60**, 1538 (2014).
- ¹⁹F. Girard, M. Antoni, S. Faure, and A. Steinchen, *Langmuir* **22**, 11085 (2006).
- ²⁰M. Born and E. Wolf, *Principles of Optics: Electromagnetic Theory of Propagation, Interference and Diffraction of Light*, 6th ed. (Pergamon, Exeter, 1980).